International Research Journal of Engineering and Technology (IRJET) e-ISSN: 2395-0056
Volume: 11 Issue: 10 | Oct 2024 www.irjet.net p-ISSN: 2395-0072

STATOR CURRENTS AND ROTOR EQUIVALENT SOURCES MODELLING AND ANALYSIS OF DFIG IN WIND ENERGY SYSTEMS

Barri Sravani[1], Prof.T.R.Jyothsna[2]

[1]*Electrical Engineering, PG scholar, Andhra University, kakaninagar, Visakhapatnam, India*
[2]*Electrical Engineering, Professor, Andhra University, Maddilapalem, Visakhapatnam, India*

ABSTRACT

The Doubly-Fed Induction Generator (DFIG) plays a critical part in present day wind vitality frameworks due to its adaptability in variable-speed applications, tall proficiency, and capability to work beneath fluctuating wind conditions. In the show situation, DFIGs are broadly utilized in wind turbines since they permit autonomous control of dynamic and receptive control, upgrading framework steadiness and vitality productivity. The variable-speed operation empowered by the rotor-side converter too makes a difference moderate mechanical stresses on the turbine, progressing generally framework reliability.

The Proportional-Integral (PI) control methodology for DFIGs, advertising a few focal points such as effortlessness, ease of usage, and vigorous execution beneath different working conditions. By controlling both stator and rotor-side voltages and streams, PI controllers proficiently oversee dynamic and receptive control stream, guaranteeing smooth network integration. The PI control approach gives steady energetic reaction, diminished motions, and improved framework execution, making it a well-known choice for both grid-connected and standalone DFIG applications.

This investigates rotor and stator current flow for torque and control, giving experiences into how successful control can optimize control yield and make strides framework steadiness. By considering these cases, the proposed control strategy illustrates made strides execution in controlling electrical amounts, accomplishing craved control stream, and minimizing unsettling influences in real-world operational scenarios.

Keywords - Small Signal Stability, DFIG, WT, RSC, GSC

I. INTRODUCTION

Energy Conversion Systems(WECS):

Overview of Wind Energy Conversion Systems(WECS):

The system to convert the kinetic energy present in the wind to useful form of energy is known as Wind Energy Conversion System(WECS). In the history, the power in the wind was exercised to give useful mechanical power but in ultramodern world WECS is substantially concentrated on conversion of energy to electrical form. There are astronomically two types of WECS – vertical axis type and perpendicular axis type. Presently, vertical axis wind turbines are the most commercially feasible for bulk power generation operations.

A WECS can be distinctly divided into three different corridor aerodynamic system, mechanical system and the electrical system as shown in figure below.

1) Aerodynamic system. The aerodynamics of the WECS system consists of wind turbine blades, turbine capitals and turbine rotor. The kinetic energy is converted into the mechanical energy in this system. likewise, utmost ultramodern wind turbine rotors are equipped with pitch servos, inside the mecca, that rotate the blades along their longitudinal axes to control the aerodynamic behavior of the blades.

2) Mechanical system. The mechanical energy attained from the kinetic energy is reused in this system. It consists of the drive- train made of a low- speed shaft coupled to the rotating mecca, a gear box (speed multiplier) that increases the low

rotational speed of the rotor to a advanced speed suitable for the electric creator, and a high- speed shaft driving the electric creator.

3) Electrical system. The mechanical energy is converted into the electrical energy in this part. It consists of the electrical creator, power transformers, grid connection.

II. EQUIVALENT FORM

Model for power system studies:

For power system studies it is common to represent generators with a simple equivalent model where by the machine is represented as a voltage source behind transient impedance, For the DFIG, the current injected to the grid is the sum of the stator current Is and grid-side converter ac-current IGSC.

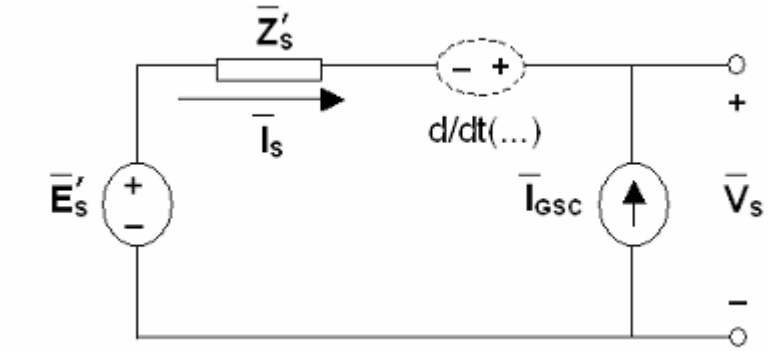

Figure 2.1: Generators as voltage source behind transient impedance

$$\frac{L'_s}{\omega_{elB}}\frac{d}{dt}i_{qs} = -R_1 i_{qs} + \omega_s L'_s i_{ds} + \frac{\omega_r e'_{qs}}{\omega_s} - \frac{e'_{ds}}{\omega_s T_r} - v_{qs} + K_{mrr} v_{qr} \quad (2.1)$$

$$\frac{L'_s}{\omega_{elB}}\frac{d}{dt}i_{ds} = -R_1 i_{ds} - \omega_s L'_s i_{qs} + \frac{\omega_r e'_{ds}}{\omega_s} + \frac{e'_{qs}}{\omega_s T_r} - v_{ds} + K_{mrr} v_{dr} \quad (2.2)$$

$$\frac{1}{\omega_s \omega_{elB}}\frac{d}{dt}e'_{qs} = R_2 i_{ds} - \frac{e'_{qs}}{\omega_s T_r} + \left(1 - \frac{\omega_r}{\omega_s}\right) e'_{ds} - K_{mrr} v_{dr} \quad (2.3)$$

$$\frac{1}{\omega_s \omega_{elB}}\frac{d}{dt}e'_{ds} = -R_2 i_{qs} - \frac{e'_{ds}}{\omega_s T_r} - \left(1 - \frac{\omega_r}{\omega_s}\right) e'_{qs} + K_{mrr} v_{qr} \quad (2.4)$$

$$i_{qr} = -\left(\frac{e'_{ds}}{X_m}\right) - K_{mrr} i_{qs} \quad (2.5)$$

$$i_{dr} = -\left(\frac{e'_{qs}}{X_m}\right) - K_{mrr} i_{ds} \quad (2.6)$$

$$\psi_{qs} = -\left(\frac{1}{\omega_s}\right) e'_{ds} - L'_s i_{qs} \quad (2.7)$$

$$\psi_{ds} = \left(\frac{1}{\omega_s}\right) e'_{qs} + L'_s i_{ds} \quad (2.8)$$

where,

$$e'_{qs} = K_{mrr}\omega_s \psi_{dr} \quad (2.9)$$

$$e'_{ds} = -K_{mrr}\omega_s \psi_{qr} \quad (2.10)$$

$$L'_s = L_{ss} - \left(\frac{L_m^2}{L_{rr}}\right) \quad (2.11)$$

$$T_r = \frac{L_{rr}}{R_r} \quad (2.12)$$

The drive train model is obtained by rearranging equations() as follows,

$$\frac{d}{dt}\omega_r = \frac{1}{2H_g}\left(k\theta_{tw} + c\frac{d}{dt}\theta_{tw} - T_e\right) \quad (2.13)$$

$$\frac{d}{dt}\theta_{tw} = \omega_{elB}(\omega_t - \omega_r) \quad (2.14)$$

$$\frac{d}{dt}\omega_t = \frac{1}{2H_t}\left(T_t - k\theta_{tw} - c\frac{d}{dt}\theta_{tw}\right) \quad (2.15)$$

The DFIG stator and rotor equivalent circuit in terms of complex variables ,the rotor voltage V_r is a controlled voltage source, which is determined by the rotor-side converter. The converter current IGSC is a controlled current source, which is determined by the grid-side converter controls.

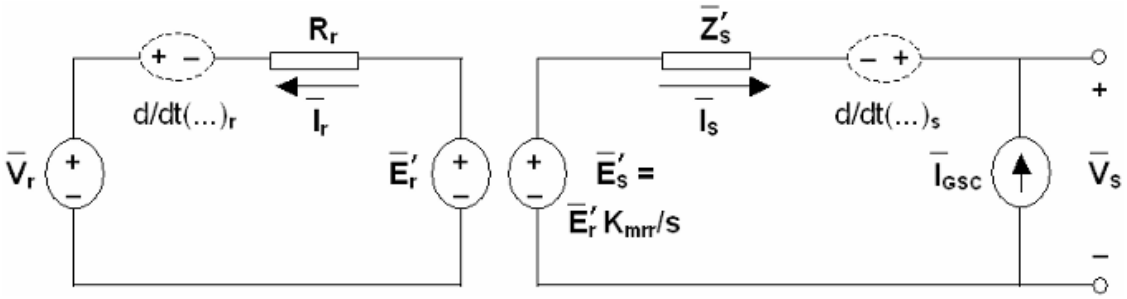

. **Figure 2.2: In detail Generators as voltage source behind transient impedance**

III. IMPLEMENTATION OF PI CONTROLLER:

RSC controls the stator reactive power and electromagnetic torque that is generated by DFIG machine. PI controller is implemented in figure below.

Rotor side converter control:

At the RSC side, the electromagnetic torque is more sensitive to i_{qr} and stator reactive power is more sensitive to idr. As shown in (31.) and (3.2), the outer loop consists torque controller where the actual value of $T_e$is compared with $T_{e,ref}$. The error is reduced to zero by the use of torque controller. Output from the torque controller is reference rotor current ($i_{qr,ref}$). Now, $i_{qr,ref}$ is compared with i_{qr} and makes the error is reduced to zero by the use of current controller. Output from this current controller is q-axis voltage (V_{qr}) that must be generated to RSC.

The implementation of pi controller for electromagnetic torque control is as follows:

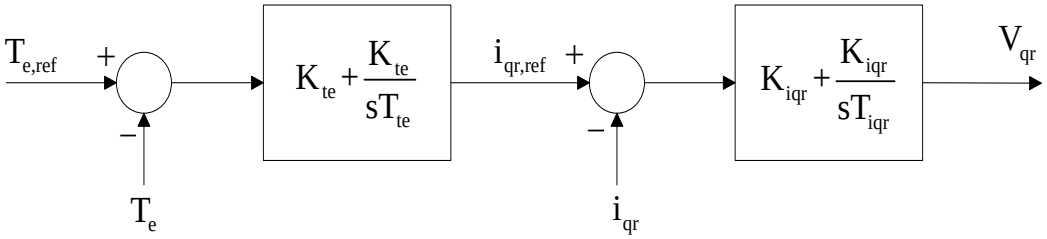

Figure 3.1: PI control loop for electromagnetic torque at RSC side

The dynamic equations of pi controller implemented for torque controller are as follows:

$$\frac{d}{dt}\phi_{te} = T_{e,err} \quad (3.1)$$

$$T_{e,err} = T_{eref} - T_e \quad (3.2)$$

$$\frac{d}{dt}\phi_{iqr} = T_{e,err}K_{te} + \frac{K_{te}}{T_{te}}\phi_{te} - i_{qr} \quad (3.3)$$

$$V_{qr} = K_{iqr}T_{e,err}K_{te} + K_{iqr}\frac{K_{te}}{T_{te}}\phi_{te} + \frac{K_{iqr}}{T_{iqr}}\phi_{iqr} - K_{iqr}i_{qr} \quad (3.4)$$

As for the reactive power is concerned (Q_s) is compared with the reference value ($Q_{s,ref}$), error is reduced to zero by integral controller action. Output from the outer control loop is $i_{dr,ref}$. Now, $i_{dr,ref}$ is compared with i_{dr} and makes the error is reduced to zero by the use of current controller. Output from this current controller is d-axis voltage (V_{dr}) that must be generated to RSC.

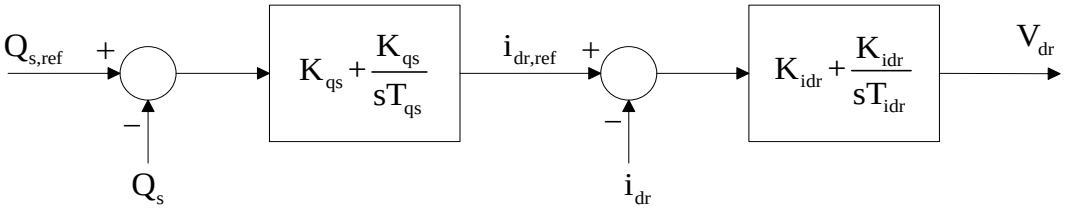

Figure 3.2: PI control loop for stator reactive power at RSC side

The dynamic equations of pi controller for stator reactive power are as follows:

$$\frac{d}{dt}\phi_{qs} = Q_{s,err} \quad (3.5)$$

$$Q_{s,err} = Q_{sref} - Q_s \quad (3.6)$$

$$\frac{d}{dt}\phi_{idr} = Q_{s,err}K_{qs} + \frac{K_{qs}}{T_{qs}}\phi_{qs} - i_{dr} \quad (3.7)$$

$$V_{dr} = K_{idr}Q_{s,err}K_{qs} + K_{idr}\frac{K_{qs}}{T_{qs}}\phi_{qs} + \frac{K_{id}}{T_{id}}\phi_{idr} - K_{idr}i_{dr} \quad (3.8)$$

The output from the current regulator, dq-axes voltage should be transferred into ABC frame. For the PWM generation of the RSC, these control voltages are used.

3.3.2 Grid-side converter and dc-link

As explained above, the GSC and dc-link dynamics are not considered in the present work.
The dc-voltage is assumed constant and the GSC is represented as a current source. It is also assumed that the GSC is operated at unity power factor. Since the GSC controls are done instantaneously, the grid-side converter ac-current is such that the active power injected to the mains matches that of the rotor-side converter at unity power factor, i.e.:

$$I_{GSC} = I_{GSCref} \quad (3.9)$$

so that 1) $P_{GSC} = Pr$ (3.10)

2) $Q_{GSC} = 0$ (3.11)

The dc-link voltage error is used to measure the imbalance. Hence by assuming instantaneous rotor active power transfer, the dc-link voltage is constant and no dynamical model is required for the dc-link capacitor. The role of the dc-link capacitor is to act as a voltage source to the converters. For drive applications using a diode rectifier on the rotor-side, the dynamics of the dc-link components may not be ignored because of the dc energy storage mechanism, bulkier dc-components, and lesser control capability . For back-to-back converters however, an adequate control eliminates the need of storage in the dc-link and ensures a practically constant dc-voltage .
When the dc-link dynamics are neglected, the model of the GSC is simply:

$$P_{GSC} = P_r \quad (3.12)$$

$$Q_{GSC} = \propto Q_{tot} \quad (3.13)$$

where $\propto$ defines the reactive power sharing between stator and GSC. For minimum converter rating, as assumed in this text, no sharing is done and $\propto = 0$, $Q_{GSC} = 0$, $Q_s = (1-\propto)Q_{tot} = Q_{tot}$. The injected current grid-side converter current is therefore $\bar{I}_{GSC} = (P_{GSC} + jQ_{GSC}) / \bar{V}_s = P_r / \bar{V}_s$.

IV. LINEARIZATION OF EACH STATES OF DFIG EQUATIONS AND ITS RESULTS

open loop states (i_{qs} , i_{ds} , e'_{qs} , e'_{ds}, ω_r, ω_t, θ_{tw}):

The 7x7 matrix constructed represents the open-loop state-space model of a doubly-fed induction generator (DFIG) connected to a wind turbine. The states in this system involve both the electrical dynamics of the DFIG and the mechanical dynamics of the wind turbine.

Closed loop states (i_{qs} , i_{ds} , e'_{qs} , e'_{ds}, ω_r, ω_t, θ_{tw} , ϕ_{iq}, ϕ_{id}, ϕ_{Te}, ϕ_{QS}):

This system consists of 11 states (11*11 matrix) equations derived from a dynamic model of a doubly-fed induction generator (DFIG)-based wind turbine system. The system integrates the dynamics of the DFIG electrical machine, the wind turbine, and controllers.

The system involves three sets of equations:

1. **DFIG Electrical Equations** (States 1-4: i_{qs} , i_{ds} , e'_{qs} , e'_{ds}):

Governed by the stator and rotor voltage equations in the q and d axes. The dynamics depend on stator/rotor inductances, resistance, mutual coupling, and rotor speed.

2. **Turbine and Mechanical Equations** (States 5-7: ω_r, ω_t, θ_{tw}):

These equations come from the mechanical torque balance, including wind power, rotor dynamics, and torsional shaft dynamics. The dynamics also consider gearbox ratios and turbine inertia.

3. **Control Equations** (States 8-11: ϕ_{iq}, ϕ_{id}, ϕ_{Te}, ϕ_{QS}):

PI controllers are used to regulate the stator currents, torque, and voltage. The control signals adjust the generator's electrical dynamics based on the desired reference values.

Eigenvalues: The eigenvalues of the matrix provide insight into the stability and dynamic response of the system. If all eigenvalues have negative real parts, the system is stable. The values indicate how fast the system's states decay or oscillate over time.

ROTOR Q-AXIS VOLTAGE (v_{qr}) and ROTOR D-AXIS VOLTAGE (v_{dr}):

$$\Delta v_{qr} = \left(-\frac{K_{iq}K_{Te}L_m e'_{qs}}{X_m} + K_{mrr}K_{iq}\right)\Delta i_{qs} + \left(-\frac{K_{iq}K_{Te}L_m e'_{ds}}{X_m}\right)\Delta i_{ds} + \left(-\frac{K_{iq}K_{Te}L_m i_{qs}}{X_m}\right)\Delta e'_{qs} + \left(-\frac{K_{iq}K_{Te}L_m i_{ds}}{X_m} + \frac{K_{iq}}{X_m}\right)\Delta e'_{ds} + \frac{K_{iq}K_{Te}}{T_{Te}}\Delta\phi_{Te} + \frac{K_{iq}}{T_{iq}}\Delta\phi_{iq}$$

$$\Delta v_{dr} = (-K_{id}K_{qs}v_{ds})\Delta i_{qs} + (K_{id}K_{qs}v_{qs} + K_{mrr}K_{id})\Delta i_{ds} + \left(-\frac{K_{id}}{X_m}\right)\Delta e'_{qs} + \frac{K_{id}K_{Qs}}{T_{Qs}}\Delta\phi_{Qs} + \frac{K_{id}}{T_{id}}\Delta\phi_{id}$$

1. i_{qs} (Stator q-axis current)

$$\frac{d}{dt}\Delta i_{qs} = \left(-\frac{\omega_{elB}R_1}{L'_s}\right)\Delta i_{qs} + \left(\frac{\omega_{elB}\omega_s L'_s}{L'_s}\right)\Delta i_{ds} + \left(\frac{\omega_{elB}\omega_r}{L'_s\omega_s}\right)\Delta e'_{qs} + \left(-\frac{\omega_{elB}}{L'_s\omega_s T_r}\right)\Delta e'_{ds} + \left(\frac{\omega_{elB}e'_{qs}}{L'_s\omega_s}\right)\Delta\omega_r + \left(-\frac{\omega_{elB}}{L'_s}\right)\Delta v_{qs} + \left(\frac{\omega_{elB}K_{mrr}}{L'_s}\right)\Delta v_{qr} \quad (4.1)$$

$$\frac{L'_s}{Welb}\frac{d}{dt}\Delta i_{qs} = \left(-R_1 - \frac{K_{mrr}K_{iq}K_{Te}L_m e'_{qs}}{X_m} + {K_{mrr}}^2 K_{iq}\right)\Delta i_{qs} + \left(\omega_s L'_s - \frac{K_{mrr}K_{iq}K_{Te}L_m e'_{ds}}{X_m}\right)\Delta i_{ds} + \left(-\frac{K_{mrr}K_{iq}K_{Te}L_m i_{qs}}{X_m} + \frac{\omega_r}{\omega_s}\right)\Delta e'_{qs} + \left(-\frac{1}{\omega_s T_r} - \frac{K_{mrr}K_{iq}K_{Te}L_m i_{ds}}{X_m} + \frac{K_{mrr}K_{iq}}{X_m}\right)\Delta e'_{ds} + \left(\frac{e'_{qs}}{\omega_s}\right)\Delta\omega_r + \frac{K_{mrr}K_{iq}K_{Te}}{T_{Te}}\Delta\phi_{Te} + \frac{K_{mrr}K_{iq}}{T_{iq}}\Delta\phi_{iq} \quad (4.2)$$

2. i_{ds} (Stator d-axis current)

$$\frac{d}{dt}\Delta i_{ds} = \left(-\frac{\omega_{elB}R_1}{L'_s}\right)\Delta i_{ds} + \left(-\frac{\omega_{elB}\omega_s L'_s}{L'_s}\right)\Delta i_{qs} + \left(\frac{\omega_{elB}\omega_r}{L'_s\omega_s}\right)\Delta e'_{ds} + \left(\frac{\omega_{elB}}{L'_s\omega_s T_r}\right)\Delta e'_{qs} + \left(\frac{\omega_{elB}e'_{ds}}{L'_s\omega_s}\right)\Delta\omega_r + \left(-\frac{\omega_{elB}}{L'_s}\right)\Delta v_{ds} + \left(\frac{\omega_{elB}K_{mrr}}{L'_s}\right)\Delta v_{dr} \quad (4.3)$$

$$\frac{L'_s}{Welb}\frac{d}{dt}\Delta i_{ds} = (-\omega_s L_s - K_{mrr}K_{id}K_{qs}v_{ds})\Delta i_{qs} + (-R_1 + K_{mrr}K_{id}K_{qs}v_{qs} + {K_{mrr}}^2 K_{id})\Delta i_{ds} + \left(\frac{1}{\omega_s T_r} - \frac{K_{mrr}K_{id}}{X_m}\right)\Delta e'_{qs} + \left(\frac{\omega_r}{\omega_s}\right)\Delta e'_{ds} + + \left(\frac{e'_{ds}}{\omega_s}\right)\Delta\omega_r + \frac{K_{mrr}K_{id}K_{Qs}}{T_{Qs}}\Delta\phi_{Qs} + \frac{K_{mrr}K_{id}}{T_{id}}\Delta\phi_{id} \quad (4.4)$$

3. (e'_{qs}) Stator q-axis transient voltage

$$\frac{d}{dt}\Delta e'_{qs} = \left(\frac{\omega_s\omega_{elB}R_2}{1}\right)\Delta i_{ds} - \left(\frac{\omega_s\omega_{elB}}{\omega_s T_r}\right)\Delta e'_{qs} + \left(\frac{\omega_s\omega_{elB}}{1}\left(1-\frac{\omega_r}{\omega_s}\right)\right)\Delta e'_{ds} - \left(\frac{\omega_s\omega_{elB}K_{mrr}}{1}\right)\Delta v_{dr}$$

. (4.5)

$$\frac{1}{\omega_s Welb}\frac{d}{dt}\Delta e'_{qs} = (K_{mrr}K_{id}K_{qs}v_{ds})\Delta i_{qs} + (-R_2 - K_{mrr}K_{id}K_{qs}v_{qs} - {K_{mrr}}^2 K_{id})\Delta i_{ds} + \left(-\frac{1}{\omega_s T_r} + \frac{K_{mrr}K_{id}}{X_m}\right)\Delta e'_{qs} + \left(1-\frac{\omega_r}{\omega_s}\right)\Delta e'_{ds} + \left(-\frac{e'_{ds}}{\omega_s}\right)\Delta\omega_r - \frac{K_{mrr}K_{id}K_{Qs}}{T_{Qs}}\Delta\phi_{Qs} - \frac{K_{mrr}K_{id}}{T_{id}}\Delta\phi_{id}$$ (4.6)

4. e'_{ds} (Stator d-axis transient voltage)

$$\frac{d}{dt}\Delta e'_{ds} = \left(-\frac{\omega_s\omega_{elB}R_2}{1}\right)\Delta i_{qs} + \left(-\frac{\omega_s\omega_{elB}}{\omega_s T_r}\right)\Delta e'_{ds} + \left(-\frac{\omega_s\omega_{elB}}{1}\left(1-\frac{\omega_r}{\omega_s}\right)\right)\Delta e'_{qs} + \left(\frac{\omega_s\omega_{elB}K_{mrr}}{1}\right)\Delta v_{qr}$$
(4.7)

$$\frac{1}{\omega_s Welb}\frac{d}{dt}\Delta e'_{ds} = \left(-R_2 - \frac{K_{mrr}K_{iq}K_{Te}L_m e'_{qs}}{X_m} + {K_{mrr}}^2 K_{iq}\right)\Delta i_{qs} + \left(-\frac{K_{mrr}K_{iq}K_{Te}L_m e'_{ds}}{X_m}\right)\Delta i_{ds} + \left(-1 - \frac{K_{mrr}K_{iq}K_{Te}L_m i_{qs}}{X_m} + \frac{\omega_r}{\omega_s}\right)\Delta e'_{qs} + \left(-\frac{1}{\omega_s T_r} - \frac{K_{mrr}K_{iq}K_{Te}L_m i_{ds}}{X_m} + \frac{K_{mrr}K_{iq}}{X_m}\right)\Delta e'_{ds} + \left(\frac{e'_{qs}}{\omega_s}\right)\Delta\omega_r + \frac{K_{mrr}K_{iq}K_{Te}}{T_{Te}}\Delta\phi_{Te} + \frac{K_{mrr}K_{iq}}{T_{iq}}\Delta\phi_{iq}$$
(4.8)

5. ω_r (Rotor speed)

$$\frac{d}{dt}\Delta\omega_r = \left(-\frac{L_m e'_{qs}}{2H_g X_m}\right)\Delta i_{qs} + \left(-\frac{L_m e'_{ds}}{2H_g X_m}\right)\Delta i_{ds} + \left(-\frac{L_m i_{qs}}{2H_g X_m}\right)\Delta e'_{qs} + \left(-\frac{L_m i_{ds}}{2H_g X_m}\right)\Delta e'_{ds} + \left(-\frac{C\,Welb}{2H_g}\right)\Delta\omega_r + \left(\frac{K}{2H_g}\right)\Delta\theta_{tw} + \left(\frac{C\,Welb}{2H_g}\right)\Delta\omega_t$$ (4.9)

6. ω_t (Turbine speed)

$$\frac{d}{dt}\Delta\omega_t = \left(\frac{\omega_{elB}c_{sh}}{2H_t}\right)\Delta\omega_r + \left(-\frac{k_{sh}}{2H_t}\right)\Delta\theta_{tw} + \frac{1}{2H_t}(-c_{sh}\omega_{elB} + L_{Wt})\Delta\omega_t$$ (4.10)

7. θ_{tw} (Torsional twist angle)

$$\frac{d}{dt}\Delta\theta_{tw} = (Welb)\Delta\omega_t + (-Welb)\Delta\omega_r$$ (4.11)

CONTROLLER EQUATIONS:

8. ϕ_{iq} (Control signal for stator q-axis current)

$$\frac{d}{dt}\Delta\phi_{iq} = K_{Te}T_{e,err} + \frac{K_{Te}}{T_{Te}}\Delta\phi_{Te} - i_{qr}$$ (4.12)

$$\frac{d}{dt}\Delta\phi_{iq} = \left(-\frac{K_{Te}L_m e'_{qs}}{X_m} + K_{mrr}\right)\Delta i_{qs} + \left(-\frac{K_{Te}L_m e'_{ds}}{X_m}\right)\Delta i_{ds} + \left(-\frac{K_{Te}L_m i_{qs}}{X_m}\right)\Delta e'_{qs} + \left(-\frac{K_{Te}L_m i_{ds}}{X_m} + \frac{1}{X_m}\right)\Delta e'_{ds} + \frac{K_{Te}}{T_{Te}}\Delta\phi_{Te}$$
(4..13)

9. ϕ_{id} (Control signal for stator d-axis current)

$$\frac{d}{dt}\Delta\phi_{id} = K_{Qs}\Delta Q_{s,err} + \frac{K_{Qs}}{T_{QS}}\Delta\phi_{QS} - \Delta i_{dr}$$ (4.14)

$$\frac{d}{dt}\Delta\phi_{id} = (-K_{qs}V_{ds})\Delta i_{qs} + (K_{qs}V_{qs} + K_{mrr})\Delta i_{ds} + \left(-\frac{1}{X_m}\right)\Delta e'_{qs} + \frac{K_{Qs}}{T_{Qs}}\Delta\phi_{Qs}$$ (4.15)

10. ϕ_{Te}(Control signal for electromagnetic torque)

$$\frac{d}{dt}\Delta\phi_{Te} = \left(-\frac{L_m e'_{qs}}{X_m}\right)\Delta i_{qs} + \left(-\frac{L_m e'_{ds}}{X_m}\right)\Delta i_{ds} + \left(-\frac{L_m i_{qs}}{X_m}\right)\Delta e'_{qs} + \left(-\frac{L_m i_{ds}}{X_m}\right)\Delta e'_{ds} \quad (4.16)$$

11. ϕ_{Qs} Control signal for stator voltage (q-axis)

$$\frac{d}{dt}\Delta\phi_{QS} = (-v_{ds})\Delta i_{qs} + (v_{qs})\Delta i_{ds} \quad (4.17)$$

OPEN LOOP TABULATED RESULTS:

Table 4.1: Base case eigenvalues of open-loop DFIG
Operating point: V_s = 1, ω_r = 1,

	$\lambda = \sigma \pm j\omega$
λ_{HF}	-16.15 ± j313.30
λ_{MF}	-10.01 ± j63.67
λ_{LF}	-0.49 ± j3.33
λ_{NO}	-17.40

HF, MF, LF =high, medium, low frequency, NO = non-oscillating.

Case 1: Sensitivity to operating point
Since the DFIG may operate at large slip with different levels of active and reactive power output, it is important to study how its dynamic behaviour changes with these conditions.

i. Rotor speed and active power
Table 4.2 shows the open-loop DFIG eigenvalues for three particular operating points. As observed above, the rotor speed has significant effect on all the eigenvalues, except for the high frequency mode. At non-synchronous speed (sub- and super-), the electrical and mechanical dynamics tend to be decoupled.

Table 4.2: Effect of rotor speed on open-loop DFIG eigenvalues
ω_r = 0.70 pu,

	$\lambda = \sigma \pm j\omega$	f_{osc}	ζ
λ_{HF}	-16.29 ± j312.91	49.80	.052
λ_{MF}	-13.18 ± j114.37	18.06	.119
λ_{LF}	-5.24 ± j7.70	1.27	.524
$ss\lambda_{NO}$	-1.24	0	1

ω_r = 1 pu,

	$\lambda = \sigma \pm j\omega$	f_{osc}	ζ
λ_{HF}	-16.15 ± j313.30	49.86	. 052
λ_{MF}	-10.01 ± j63.67	10.13	. 155
λ_{LF}	-0.49 ± j3.33	0.53	. 138
λ_{NO}	-17.40	0	1

ω_r = 1.29 pu,

	$\lambda = \sigma \pm j\omega$	f_{osc}	ζ
λ_{HF}	-16.29 ± j312.91	49.90	.051
λ_{MF}	-13.18 ± j114.37	17.55	.151
λ_{LF}	-5.24 ± j7.70	1.48	.243
λ_{NO}	-1.24	0	1

Case 2: Sensitivity to machine parameters

In this subsection the effect of machine inductances (L_{ss}, L_{rr} and L_m), resistances (R_s and R_r) and mechanical parameters (H_g, H_t and k) on the eigenvalues of the open-loop DFIG are observed. These parameters vary with the size of the machine, the design, the materials used, and the working conditions (e.g. higher temperature). The range of parameter values may be large. It is therefore worthwhile to examine how the dynamics are affected and whether some particular values lead to instability. In this subsection, all eigenvalues are obtained for the base case operating point, i.e. nominal terminal voltage and synchronous rotor speed (V_s = 1 pu, w_r = 1 pu).

i. Inductances

The machine inductances have significant effect on the stability of the open-loop DFIG. For some values, the open-loop DFIG at zero slip is unstable. For the discussion, it is useful to define the ratio of stator self to mutual inductance $a_{ss} = L_{ss} / L_m$,the ratio of rotor self to mutual inductance $a_{rr} = L_{rr} / L_m$, and the 'transient stator inductance' $L'_S = L_{SS} - L_m^2/L_{rr} = L_m(a_{ss} - 1/a_{rr})$ Table 4.3 shows the eigenvalues of the open-loop DFIG at zero slip for different ratios a_{ss} and a_{rr} with mutual inductance L_m = 4 pu.

The machine is stable (all eigenvalues with negative real part) for $L'_s \geq 0.01$. Alternatively, a more restrictive stability condition is that both $a_{ss} \geq 1$ $a_{rr} \geq 1$ i.e. both $L_{ss} \geq L_m$ and $L_{rr} \geq L_m$, which means that leakage inductances are positive as explained below. When the magnitude of $L's$ is small i.e. when $a_{ss}a_{rr} \approx 1$($L_{ss} \approx L_m$ and $L_{rr} \approx L_m$) the eigenvalue sensitivity is larger and there is more coupling between the modes .

Table 4.3: Effect of stator and rotor inductances on the modes of the open-loop DFIG at zero slip $a_{ss} = L_{ss} / L_{m,}$, $a_{rr} = L_{rr} / L_m$, L_m = 4 pu, $L'_s = L_m(a_{ss}\text{-}1/a_{rr})$

a_{ss}	a_{rr}	L'_s	λ_{HF}	λ_{MF}	λ_{NO}	λ_{LF}
1.01	1.130	+0.5	-3.15 ± j 314.1	-3.33 ± j29.9	-3.09	-0.41 ± j3.16
1.01	1.003	+0.05	--31.5 ± j310.9	-16.9 ± j86.9	-33.87	-0.50 ± j3.35
1.01	0.991	+0.003	-807.0 ± j157.4	8.03 ± j187.0	-219.51	-0.51 ± j3.37
1.01	0.989	-0.004	+761.2 ± j113.0	52.04 ± j195.1	-144.12	-0.51 ± j3.37
1.01	0.978	-0.05	+30.16 ± j310.5	36.29, 107.9	-73.6	-0.52 ± j3.40
1.01	0.881	-0.5	+3.12 ± j314.1	3.97, 26.9	-26.1	-0.64 ± j3.62
0.99	1.156	+0.5	-3.15 ± j314.1	-3.28 ± j29.9	-2.96	-0.40 ± j3.16
0.99	1.023	+0.05	-32.8 ± j310.8	-16.8 ± j88.7	-33.8	-0.49 ± j3.35
0.99	1.011	+0.003	-826.10 ± j161.0	8.96 ± j185.5	-222.35	-0.50 ± j3.37
0.99	1.009	-0.004	775.5 ± j115.8	52.24 ± j192.6	-147.2	-0.50 ± j3.38
0.99	0.998	-0.05	31.3 ± j310.3	36.3, 109.7	-75.3	-51 ± j3.40
0.99	0.897	-0.5	3.13 ± j314.1	3.83, 26.8	-26.2	-0.62 ± j3.62

The parameter L_s must be different from zero in order for i_{qs} and i_{ds} to be state variables (if L'_s = 0, the variable i_{qs} and i_{ds} are algebraic variables i.e. there is no stator transients). When $L's \neq 0$, the first two diagonal entries of the state matrix are $A_{sys}(1,1) = A_{sys}(2,2) = -R_1 w_{el}/L'_s$. The diagonal elements of the state matrix are the centers of the Gershgorin disks which contain the eigenvalues of the matrix. Hence for positive L'_s, the centers of the first two Gershgorin disks, are in the left half plane. For negative L'_s, the disk centers are in the right half plane. As L'_s is in the denominator, the displacement in the disk centers and hence the sensitivity of the eigenvalue location with respect to L'_s is larger for small amplitude of L'_s.

In the above discussion, the effect of varying the ratios a_{ss} and a_{rr} for a given value of mutual inductance L_m was examined. Table 4.4 shows the effect of varying L_m with constant ratio a_{ss} = 1.01 and a_{rr} = 1.015. The eigenvalues in which electrical state variables participate (λ_{HF}, λ_{MF}, λ_{NO}) are mostly affected. For all modes, when Lm decreases, the real part magnitude increases while the imaginary part magnitude changes also but to a lesser extent. Since L_m is inversely related to the airgap length, this means that for larger airgap machine (smaller L_m), time constants decrease and damping ratios increase.

Table 4.4: Effect of mutual inductance on the modes of the open-loop DFIG at zero slip
L_m in [pu], a_{ss} = 1.01, a_{rr} = 1.015, $L'_s = L_m(a_{ss}-1/a_{rr})$

L_m	L'_s	λ_{HF}	λ_{MF}	λ_{NO}	λ_{LF}
10	0.247	-6.39 ± j314.0	-5.15 ± j41.23	-6.96	-0.46 ± j3.26
8	0.198	-8.00 ± j313.9	-5.98 ± j45.78	-8.70	-0.47 ± j3.28
6	0.148	-10.71 ± j313.7	-7.35 ± j52.48	-11.61	-0.48 ± j3.30
4	0.099	-16.18 ± j313.2	-10.02 ± j63.72	-17.43	-0.49 ± j3.33
2	0.049	-33.11 ± j310.6	-17.43 ± j89.02	-35.12	-0.49 ± j3.35
1	0.024	-70.24 ± j300.0	-28.3 ± j125.01	-71.86	-0.50 ± j3.36

ii. Resistances

Varying the stator and rotor resistance while keeping all other parameters constant causes noticeable displacement in eigenvalues and change in participation factors. For the discussion, the ratio of the rotor to stator resistance is defined as $a_r = R_r/R_s$. Table 4.5 shows the eigenvalues of the open-loop DFIG at zero slip for different values of stator resistance R_s with $a_r > 1$ and < 1.

Table 4.5: Effect of stator and rotor resistance on the modes of the open-loop DFIG at zero slip
R_s in [pu], $a_r = R_r/R_s$ (L_m = 4 pu, a_{ss} = 1.01, a_{rr} = 1.015)

R_s	a_r	Eigenvalues			
0.0001	1.1	-0.32 ± j314.1	-2.13 ± j64.02	-0.25 ± j3.37	-0.34
0.005	1.1	-16.18 ± j313.29	-10.02 ± j63.72	-0.49 ± j3.33	-17.43
0.05	1.1	-205 ± j153.35	-112.36 ± j159.94	-2.79 ± j2.18	-27.46
0.1	1.1	-616 ± j150.3	-40.89 ± j163.4	-7.92 ± j7.53	-2.36
0.0001	0.9	-0.32 ± j314.15	-2.10 ± j64.01	-0.251 ± j3.37	-0.28
0.005	0.9	-16.19 ± j313.46	-8.49 ± j63.85	-0.44 ± j3.34	-14.26
0.05	0.9	-182.18 ± j220.6	-98.58 ± j92.96	-2.24 ± j2.63	-39.25
0.1	0.9	-548.98 ± j169.5	-43.88 ± j144.34	-9.29 ± j5.04	-1.79

For the tested range of parameters, the system is stable. For larger resistance values, the real part magnitude of complex conjugate modes tends to be larger (i.e. oscillating modes are further away from the imaginary axis when resistances are larger). Hence more resistive machines have oscillatory dynamics with smaller time constants. For very resistive machines ($R_s \geq 0.1$), the real mode is the dominant mode (closest to the imaginary axis) and the system is referred to as over-damped.

For more resistive machines, the electrical and mechanical dynamics are decoupled, as shown in Table 4.6, where for R_s = 0.1, λ_{HF1} and λ_{HF2} are electrical modes, λ_{LF} and λ_{NO} are mechanical modes.

Table 4.6: open-loop DFIG at zero slip for different resistances
R_s =0.1pu (a_r =1.1, L_m =4pu, a_{ss} =1.01, a_{rr} = 1.015)

	$\lambda = \sigma \pm j\omega$
λ_{HF}	-616.63 ± j150.39
λ_{MF}	-40.90 ± j163.46
λ_{LF}	-7.9 ± j7.53
λ_{NO}	-1.39

R_s =0.0001pu (a_r =1.1, L_m =4pu, a_{ss} =1.01, a_{rr} = 1.015)

	$\lambda = \sigma \pm j\omega$
λ_{HF}	-0.32 ± j314.15
λ_{MF}	-2.13 ± j63.18
λ_{LF}	-0.25 ± j1.05
λ_{NO}	-0.34

iii. Mechanical parameters

Table 4.7 shows the effect of varying inertias and stiffness on the open-loop DFIG eigen values. As expected, heavier machines (large H_t and H_g) present oscillations with lower frequencies, and drive trains that are stiffer (smaller gearbox ratio i.e. larger k) have oscillations with higher frequencies.

Table 4.7: Effect of drive train parameters on the modes of the open-loop DFIG at zero slip

H_t in [s], $H_g = 0.1H_t$, $k = 0.3$pu

H_t	λ_{HF}	λ_{MF} (f_{osc}[HZ], ζ)	λ_{LF} (f_{osc}[HZ], ζ)	λ_{NO}
12	-15.92 ± j313.3	-8.91 ± j36.06 (5.75,.239)	-0.32 ± j1.92 (0.31,.168)	-17.39
8	-15.97 ± j313.3	-9.19 ± j44.59 (7.11,.201)	-0.36 ± j2.35 (0.37,.155)	-17.40
4	-16.15 ± j313.3	-10.00 ± j63.66 (10.2,.155)	-0.49 ± j3.33 (0.53,.146)	-17.40
2	-16.51 ± j313.2	-11.61 ± j90.42 (14.4,.123)	-0.73 ± j4.70 (0.75,.155)	-17.40
1	-17.36 ± j313.2	-14.72 ± j128.0 (20.4,.114)	-1.22 ± j6.62 (1.05,.182)	-17.40

k in[pu], H_t = 4 s, Hg = 0.1H_t

For the tested range of parameters, the machine dynamics remain stable. The electrical modes (high frequency and non-oscillating modes) are not significantly sensitive to mechanical parameters.

k	λ_{HF}	λ_{MF} (f_{osc}[HZ], ζ)	λ_{LF} (f_{osc}[HZ], ζ)	λ_{NO}
30	-16.19± j313.30	-3.71± j128.89 (20.5,.029)	-6.74 ± j15.43 (2.47,.398)	-17.37
3	-16.15 ± j313.30	-8.28 ± j71.53 (11.4,.115)	-2.21 ± j9.27 (1.48,.231)	-17.39
.3	-16.15 ± j313.30	-10.00 ± j63.66 (10.2,.155)	-0.49 ± j3.33 (0.53,.146)	-17.40
.03	-16.15 ± j313.30	-10.21 ± j62.85 (10.0,.160)	-0.27 ± j1.04 (0.17,.260)	-17.40
.003	-16.15 ± j313.30	-10.24 ± j62.77 (10.0.160)	-0.25 ± j0.22 (0.04,.758)	-17.40

CLOSED LOOP TABULATED RESULTS:

Case 1: Closed-loop DFIG eigenvalues

To facilitate the discussion, the typical eigenvalues of a closed-loop DFIG with properly tuned controls are first presented and compared with those of the open-loop case. The tuning method of the rotor side converter PI controllers is discussed in detail subsequently.

Table 4.8 shows the typical eigenvalues of a well-tuned closed-loop DFIG. Details on the determination of the control parameters are given in the next subsections. The following eigenvalues can be distinguished:

Stator modes (i_{qs} , i_{ds})

Rotor flux modes (e'_{qs} , e'_{ds})

Turbine modes (ω_r , θ_{tw} , ω_t)

Controller modes (Φ_{iq} , Φ_{id} , Φ_{Te} , Φ_{qs})

TABLE 4.8: Eigenvalues of the DFIG with closed controls

q-axis gains: K_{Te} = -1.5 T_{Te} = 0.250 K_{iq} = -1 T_{iq} = 0.0250

d-axis gains: K_{Qs} = 1 T_{Qs} = 0.50 K_{id} = -0.5 T_{id} = 0.050

$\lambda = \sigma \pm j\omega$	Dominant states
-7826.19	i_{qs}
-3144.10	i_{ds}
-0.15 $\pm j$ 313.39	e'_{qs} e'_{ds}
-2.14 $\pm j$ 11.11	ω_r θ_{tw}
-0.11	ω_t
-40.67	Φ_{iq}
-20.01	Φ_{id}

-2.39	Φ_{Te}
-0.99	Φ_{qs}

The stator modes are real and have large magnitude. The location of the stator eigen values depend on machine parameters, operating point and indeed control parameters. As explained later, they are either far in the LHP or far in the RHP. The control parameters can be chosen so that the stator modes are placed at some desired location. Limit values for the controller proportional gains can be determined to ensure that the stator modes are in the LHP (see next subsection). It is noted that large magnitudes for the stator eigenvalues are not a problem (the problem is a positive sign as it means instability). In fact, large negative real part is desirable since in such case the eigenvalue can be considered to be at (relatively to the other eigenvalues) so that stator transients can be neglected i.e. so that stator variables can be approximated as algebraic variables instead of state variables (differential variables).

The rotor-flux mode is a high-frequency oscillating mode (40~55 Hz). It is sensitive to the model order (neglecting stator transients changes the location of this mode) and controller parameters. If the controllers are not tuned properly, this mode is in the RHP. Limit values for the proportional gains can also be determined to ensure that the rotor f lux is stable (see next subsection). It is seen that the high frequency mode (50 Hz) is due to the rotor electrical dynamics. This is in contrast with the familiar result for the synchronous generator, squirrel-cage induction generator and open-loop DFIG where the 50 Hz mode is associated with stator dynamics. For the closed-loop DFIG, neglecting stator transients does not remove the 50 Hz mode, though it increases slightly its damping.

The controller modes may be real or highly damped complex-conjugates depending on the control parameters. They may also be coupled with the generator or drive train dynamics depending on the control parameters.

From the observations, the closed-loop system differs from the open-loop configuration in several aspects. Apart from introducing controller modes and changing the coupling of the machine dynamics (no electro-mechanical mode for the closed-loop system), an important consequence of the converter controllers is that stator dynamics are associated with large real eigenvalues while the 50 Hz mode is associated with rotor electrical dynamics. As rotor electrical dynamics are not significantly coupled with the other dynamics, both stator and rotor electrical dynamics should be neglected if the point of interest is in low frequency oscillations as for power system stability studies (neglecting stator transients only does not remove the 50 Hz oscillations).

4.5.1 Tuning issues of rotor-side converter
For each PI controller), the parameters K and T (proportional gains and integral times) have to be selected for stability and desired performance. Root-loci plots show that stability of the closed-loop DFIG is mainly decided by the proportional gains (P-gains), while the integral times (I-times) influence mainly the speed of integral action. In this section, the particular issues relating to stability are examined, hence the discussion focusses on the P-gains. The effect of the I-times is reviewed in the next section.

Below, there are DFIG models are considered:
Full-order model (FOM)
5th order model (5thOM): stator transients neglected
3rd order model (3rdOM): stator and rotor electrical transients neglected
We considered the Full-order model (FOM) in experimental through controller.

In the full-order model, all electrical dynamics (stator and rotor) change with a finite speed, and the DFIG has seven state variables (i_{qs}, i_{ds}, e_{qs}, e_{ds}, ω_r , θ_{tw} , ω_t). In the 5th order model, the stator variables are considered as algebraic, in other words they are assumed to change instantaneously; the DFIG has five state variables (e_{qs}, e_{ds}, ω_r , θ_{tw} , ω_t). In the 3rd order model, all electrical variables are considered as algebraic, and the DFIG has three state variables representing the mechanical dynamics (ω_r , θ_{tw} , ω_t). Since there are four controller states (Φ_{iq} , Φ_{id} , Φ_{Te} , Φ_{qs}), the model order of the closed-loop DFIG(number of DFIG states + number of controller states) is 11, 9 and 7 for the FOM, 5th OM and 3rd OM respectively.

4.5.2 Inappropriate tuning with simplified DFIG model

One particularity of the DFIG is that when tuning the controllers with the 5th or 3rd OM, one may obtain a set of PI-gains giving stable results for the reduced order models, but unstable for the full order model.

4.9 Example of inadequate PI gains and corresponding eigen values
q-axis gains: K_{Te} = -1.5 T_{Te} = 0.250 K_{iq} = -1 T_{iq} = 0.0250
d-axis gains: K_{Qs} = 1 T_{Qs} = 0.50 K_{id} = -0.5 T_{id} = 0.050

$\lambda = \sigma \pm j\omega$	Dominant states
+171970.99	i_{qs}
-901.82	i_{ds}
+1.14 $\pm j$ 313.21	e'_{qs} e'_{ds}
-2.13 $\pm j$ 11.18	ω_r θ_{tw}
-0.11	ω_t
-399.04	Φ_{iq}
-267.61	Φ_{id}
-36.33	Φ_{Te}
-32.67	Φ_{qs}

In Table 4.9, the DFIG is stable if stator or both stator and rotor electrical transients are neglected . However, the DFIG is unstable if both stator and rotor electrical transients are considered (FOM) in which case the rear two eigen values in the RHP. In other words, if stator variables change instantaneously, the DFIG is stable; if however, stator dynamics have a small but non-zero time constant (which is more likely to Both case in the real system), the DFIG is unstable. This is undesirable asstability is sensitive to model order and only guaranteed in the ideal case where stator or both stators.

4.5.3 Stator mode's location: Limit value of the P-gains

The location of the stator modes can be evaluated analytically by applying Gershgorin theorem [130] on the state matrix of the closed-loop grid connected DFIG. Gershgorin theorem states that the eigenvalues of a matrix A are located in the union of the disks in the complex plane which have as centre the diagonal elements of A and as radius the sum of the off-diagonal elements (either row-wise or column-wise) [130]. Hence if all diagonal elements have negative real part, all disks are centered in the LHP and the eigenvalues are more likely to be in the LHP.

For the closed-loop DFIG full order model, the diagonal elements of the state matrix corresponding to the differential equations of the stator states (i_{qs} and i_{ds}) are:

$$a_{11} = \left(-R_1 + K_{mrr}K_{iq}\left(K_{mrr} - K_{Te}\frac{e'_{qs0}}{w_s}\right) - \left[\frac{\partial v_{qs}}{\partial i_{qs}}\right]_0\right)\left(\frac{Wel}{L'_s}\right) \quad (4.18)$$

$$a_{22} = \left(-R_1 + K_{mrr}K_{id}\left(K_{mrr} - K_{vs}\left[\frac{\partial v_{qs}}{\partial i_{ds}}\right]_0\right) - \left[\frac{\partial v_{ds}}{\partial i_{ds}}\right]_0\right)\left(\frac{Wel}{L'_s}\right) \quad (4.19)$$

Where $\partial v_{qs}/\ i_{qs}$, $\partial v_{qs}/\ \partial i_{ds}$ and $\partial v_{ds}/\ \partial i_{ds}$ depend on the external network. Obtaining an analytical expression for these terms is not readily feasible. In a first step they can be ignored, which is the same as assuming constant terminal voltage (i.e. the DFIG is connected to an infinitely strong system). The effect of non-constant terminal voltage can be checked subsequently with numerical computation of the eigenvalues and time domain simulations. Hence:

$$a_{11} \approx \left(-R_1 + k_{mrr}^2 K_{iq} - K_{mrr}K_{iq}K_{Te}\frac{e'_{qs0}}{w_s}\right)\left(\frac{Wel}{L'_s}\right) \quad (4.20)$$

$$a_{22} \approx \left(-R_1 + k_{mrr}^2 K_{id} + K_{mrr}K_{id}K_{Q_s V_{qs0}}\right)\left(\frac{Wel}{L'_s}\right) \quad (4.21)$$

It is seen that a_{11} and a_{22} depend on the operating point (v_{qs0}, e'_{qs0}), the machine parameters (R_1, K_{mrr}, L'_s), and the P-gains (K_{iq}, K_{id}, K_{Te}, K_{Qs}). The dynamics of the DFIG are such that the stator eigenvalues are relatively closer to a_{11} and a_{22} than to the other diagonal elements of the state matrix. In Gershgorin framework, this is because a transformation can be applied to the state matrix so that the disks centered at a_{11} and a_{22} are disconnected from the remaining disks

In other words, one can obtain a set of P-gains for some desired location of a_{11} and a_{22}, i.e. one can place the stator modes in some desired region of the left half plane around a_{11} and a_{22} by choosing the P-gains appropriately. E.g. for the q-axis stator mode to be in the LHP around -T_1 where T_1 is real positive, i.e. for the condition $a_{11} \leq -T_1$ to be satisfied, the threshold value (minimum or maximum) of the proportional gain K_{Te} can be obtained using (4.118) as:

If $k_{iq} > 0$ and $e'_{qs0} > 0 \rightarrow K_{Te} \geq K_{Te,th}$
If $k_{iq} > 0$ and $e'_{qs0} < 0 \rightarrow K_{Te} \leq K_{Te,th}$
If $k_{iq} < 0$ and $e'_{qs0} > 0 \rightarrow K_{Te} \leq K_{Te,th}$ (4.22)
If $k_{iq} < 0$ and $e'_{qs0} < 0 \rightarrow K_{Te} \geq K_{Te,th}$

Where,

$$K_{Te,th} = \left(\frac{1}{K_{iq}K_{mrr}}\left(\frac{L'_sT_1}{Wel} - R_1\right) + K_{mrr}\right)\left(\frac{w_s}{e'_{qs0}}\right) \quad (4.23)$$

Similarly, for the d-axis stator mode to be in the LHP around -T2 whereT2 is real positive, i.e. for the condition $a_{22} \leq -T_2$ to be satisfied, one can obtain the threshold value of the proportional gain K_{Qs} using (4.119) as:

If $k_{id} > 0 \rightarrow K_{Qs} \leq K_{Qs,th}$
If $k_{id} < 0 \rightarrow K_{Qs} \geq K_{Qs,th}$ (4.24)

Where

$$K_{Qs,th} = \left(\frac{1}{K_{id}K_{mrr}}\left(\frac{L'_sT_2}{Wel} + R_1\right) - K_{mrr}\right)\left(\frac{1}{v_{qs0}}\right) \quad (4.25)$$

Equations (4.120)-(4.123) give restrictions on the outer loop P-gains for some T_1 and T_2 as function of inner loop P-gains and operating point. As the integral time of the current controllers is in the order of milliseconds , a consistent choice for T_1 and T_2 is $T_1 = T_2$ =10000 which gives a time constant for the stator modes in the order of 1/10000 = 0.1 ms i.e. ten times faster than the current controller integral action (stator transients should be faster so that they can be neglected).

4.5.4 Robustness verification:

The above analysis describes the dynamics around a particular operating point for some machine parameters and small disturbances. In this section, the effect of changing para meters and conditions on the eigenvalues of the closed-loop DFIG is examined.

i. Robustness to operating point

Table 4.10: Effect of rotor speed on the closed-loop DFIG Modes

ω_r	λ_{iqs}	λ_{ids}	$\lambda_{e'_{qs}\ e'_{ds}}$	$\lambda_{\omega_r\ \theta_{tw}}$	λ_{ω_t}
0.7	-7824.33	-3146.05	-0.15 $\pm j$ 313.66	-2.14$\pm j$11.11	-0.11
0.8	-7825.39	-3144.95	-0.15 $\pm j$ 313.56	-2.14$\pm j$11.11	-0.11
0.9	-7826.02	-3144.29	-0.15 $\pm j$ 313.45	-2.14$\pm j$11.11	-0.11
1.0	-7826.24	-3144.05	-0.15 $\pm j$ 313.34	-2.14$\pm j$11.11	-0.11
1.1	-7826.03	-3144.23	-0.16 $\pm j$ 313.23	-2.14$\pm j$11.11	-0.11
1.2	-7825.40	-3144.84	-0.16 $\pm j$ 313.12	-2.14$\pm j$11.11	-0.11

$\lambda_{\Phi_{iq}}$	$\lambda_{\Phi_{id}}$	$\lambda_{\Phi_{Te}}$	$\lambda_{\Phi_{qs}}$
-40.62	-19.99	-2.39	-0.99
-40.65	-19.99	-2.39	-0.99
-40.66	-20.00	-2.39	-0.99
-40.68	-20.01	-2.39	-0.99
-40.68	-20.02	-2.39	-0.99
-40.68	-20.04	-2.39	-0.99

For table 4.10 different rotor speeds, the only noticeable variation is in the mechanical turbine mode, which is closer to the imaginary axis for synchronous and super-synchronous speed but remains stable. This means that for w_r the rotational speed takes longer to reach anew steady state value.

Table 4.11 show the effect of the terminal voltage and reactive power level on the closed-loop DFIG modes. Again, the dynamical characteristics of the system are preserved over the wide range of tested conditions.

Table 4.11 : Effect of terminal voltage on closed-loop DFIG modes

v_s	λ_{iqs}	λ_{ids}	$\lambda_{e'_{qs}\ e'_{ds}}$	$\lambda_{\omega_r\ \theta_{tw}}$	λ_{ω_t}
1.1	-7826.20	-3299.90	-0.14 $\pm j$ 313.42	-2.14$\pm j$11.11	-0.11
1.0	-7826.20	-3144.10	-0.15 $\pm j$ 313.38	-2.14$\pm j$11.11	-0.11
0.9	-7826.20	-2988.30	-0.16 $\pm j$ 313.35	-2.14$\pm j$11.11	-0.11
0.8	-7826.20	-2832.50	-0.18 $\pm j$ 313.31	-2.14$\pm j$11.11	-0.11
0.75	-7826.20	-2754.60	-0.18 $\pm j$ 313.28	-2.14$\pm j$11.11	-0.11
0.5	-7826.20	-2365.13	-0.22 $\pm j$ 313.15	-2.14$\pm j$11.11	-0.11

$\lambda_{\Phi_{iq}}$	$\lambda_{\Phi_{id}}$	$\lambda_{\Phi_{Te}}$	$\lambda_{\Phi_{qs}}$
-40.67	-20.01	-2.39	-1.04
-40.67	-20.01	-2.39	-0.99
-40.67	-20.01	-2.39	-0.94
-40.67	-20.01	-2.39	-0.88
-40.67	-20.01	-2.39	-0.85
-40.67	-20.01	-2.39	-0.66

ii. Robustness to machine parameters

Table 4.12 and 4.13 give the closed-loop DFIG eigenvalues with the gains for different machine inductances and resistances.

4.12: Effect of inductances on the closed-loop DFIG modes

Control parameters of Table 4.12 are used; L_{ss}=1.01Lm ; L_{rr} = 1.005 L_{ss}

L_m	λ_{iqs}	λ_{ids}	$\lambda_{e'_{qs}\ e'_{ds}}$	$\lambda_{\omega_r\ \theta_{tw}}$	λ_{ω_t}
8	-3890.48	-1562.22	-0.11 $\pm j$ 313.39	-2.14$\pm j$11.11	-0.11
6	-5202.57	-2089.40	-0.12 $\pm j$ 313.39	-2.14$\pm j$11.11	-0.11
4	-7826.19	-3144.10	-0.15 $\pm j$ 313.39	-2.14$\pm j$11.11	-0.11
2	-15695.9	-6308.89	-0.30 $\pm j$ 313.39	-2.14$\pm j$11.11	-0.11
1	-31434.6	-12638.9	-0.64 $\pm j$ 313.39	-2.14$\pm j$11.11	-0.11

$\lambda_{\Phi_{iq}}$	$\lambda_{\Phi_{id}}$	$\lambda_{\Phi_{Te}}$	$\lambda_{\Phi_{qs}}$
-40.90	-20.14	-2.391	-0.995
-40.78	-20.07	-2.391	-0.995
-40.67	-20.01	-2.391	-0.995
-40.56	-19.94	-2.391	-0.995
-40.50	-19.91	-2.392	-0.995

It is seen that for the wide range of values considered, the dynamical characteristics of the system are preserved. The electrical modes are sensitive to the variation of inductances and resistances. For high inductances, the magnitude of the stator modes are reduced but they remain far from the current controller modes in the LHP. For different resistances, the DFIG modes are virtually unchanged when resistances are small. In very resistive machine, the 50 Hz mode (rotor flux mode) has a lower damping ratio. Retuning of the controllers may be required to keep the damping ratio at an acceptable level.

Table 4.13: Effect of resistances on the closed-loop DFIG modes
Control parameters of Table 5.5 are used; R_r=1.1R_s

R_s	λ_{iqs}	λ_{ids}	$\lambda_{e'_{qs}\ e'_{ds}}$	$\lambda_{\omega_r\ \theta_{tw}}$	λ_{ω_t}
.0001	-7793.71	-3111.75	-0.0031 $\pm j$ 314.14	-2.14$\pm j$11.11	-0.11
.001	-7799.67	-3117.69	-0.031 $\pm j$ 314.00	-2.14$\pm j$11.11	-0.11
.01	-7859.34	-3177.12	-0.31 $\pm j$ 312.63	-2.14$\pm j$11.11	-0.11
.05	-8124.48	-3441.27	-1.55 $\pm j$ 307.05	-2.14$\pm j$11.11	-0.11
.1	-8455.74	-3771.49	-3.06 $\pm j$ 301.02	-2.14$\pm j$11.11	-0.11

$\lambda_{\Phi_{iq}}$	$\lambda_{\Phi_{id}}$	$\lambda_{\Phi_{Te}}$	$\lambda_{\Phi_{qs}}$
-40.77	-20.13	-2.388	-0.995
-40.75	-20.11	-2.389	-0.995
-40.57	-19.89	-2.394	-0.995
-39.80	-18.96	-2.419	-0.998
-38.89	-17.92	-2.448	-1.001

Table 4.14 gives the closed-loop DFIG modes for different inertias. The mechanical modes are sensitive to the variation of inertias. For heavier machines, the mechanical dynamics are slower (smaller real part magnitude) as expected but remain stable.

Table 4.14: Effect of inertias on the closed-loop DFIG modes Control parameters of Table 5.5 are used; H_g=0.1Ht

H_g	λ_{iqs}	λ_{ids}	$\lambda_{e'_{qs}\ e'_{ds}}$	$\lambda_{\omega_r\ \theta_{tw}}$	λ_{ω_t}
12	-7826.54	-3144.10	-0.158 $\pm j$ 313.39	-0.716$\pm j$ 6.52	-0.037
8	-7826.45	-3144.10	-0.158 $\pm j$ 313.39	-1.074$\pm j$ 7.95	-0.056
6	-7826.37	-3144.10	-0.158 $\pm j$ 313.39	-1.431$\pm j$ 9.14	-0.075
3	-7826.02	-3144.10	-0.157 $\pm j$ 313.39	-2.856$\pm j$ 12.72	-0.151
1	-7824.66	-3144.10	-0.155 $\pm j$ 313.39	-8.476$\pm j$ 20.48	-0.455

λ_{ω_t}	$\lambda_{\Phi_{iq}}$	$\lambda_{\Phi_{id}}$	$\lambda_{\Phi_{Te}}$	$\lambda_{\Phi_{qs}}$
-0.037	-40.30	-20.01	-2.394	-0.995
-0.056	-40.39	-20.01	-2.393	-0.995
-0.075	-40.48	-20.01	-2.392	-0.995
-0.151	-40.86	-20.01	-2.390	-0.995
-0.455	-42.56	-20.01	-2.380	-0.995

V. CONCLUSION

In this Work the wind driven DFIG model was been presented. Model equations were been derived and parameters data of each component were provided. For the turbine, dynamic models (aerodynamics of the airflow around the turbine) are used for turbine design or specific site-turbine evaluation.

For power system model stability studies, where the mechanical input power is obtained from the wind speed, pitch angle and rotor speed. A procedure has been given for consistent dimension calculation when using numerical approximations with Cp curve. In such case, the drive train does not behave as a single equivalent rotating mass. In addition to evaluate the control performance accurately, it is important to consider the change in rotor speed as realistically as possible. Hence the two mass-model is used.

For the induction generator, the derivation of the model equations has been presented to define unambiguously all parameters, variables and conventions used in the present work. For power system model studies, the DFIG can be represented as a voltage source (proportional to rotor flux) behind transient impedance, with a shunt controlled current source at the terminal representing the current from the grid-side converter. Detailed explanation for the per unit conversion had been done in this work and choice of the base values have been given.

For the ac-dc-ac converter, the grid side converter controls are assumed as ideal i.e. the dc-voltage is constant (hence dc-link dynamics are ignored) and the GSC transfers the rotor active power instantaneously to or from the grid. It is also assumed that the GSC is operated at unity power factor. The RSC on the other hand is modelled as a controlled voltage source. The rotor voltage setpoints are determined by two loops of PI-controllers in cascade regulating the electrical torque and reactive power. Switching transients were ignored and rotor voltages are instantaneously equal to their setpoints.

VI. REFERENCES

[1]. F. Mei, B.C. Pal, "Modal Analysis of a Grid Connected Doubly-Fed Induction Generator," in Proc. of Power Electronics, Machines and Drives Int. Conf., April 2006, pp 611-615. F.

[2]. Mei, B.C. Pal, "Modelling and dynamic behavior of wind generation as it re lates to power system control and dynamic performance," in Cigre Technical Report Working Group 601 of Study Committee C4, CIGRE-WG-601.C4, Chapter contribution, January 2007.

[3]. F. Mei, B.C. Pal, "Modal analysis of grid connected doubly-fed induction generators," in IEEE trans. on Energy Conversion, vol 22, nb 3, September 2007, pp 728-736. F. Mei, B.C. Pal, "On the modelling adequacy of the DFIG in power system stability studies," in IET Journal of Renewable Power Generation, vol 2, nb 3, September 2008, pp 181-190.

[4]. Boldea, Variable Speed Generators. CRC Press Taylor & Francis, 2006. Boldea and A. Nasar, The Induction Machine Handbook. CRC Press, 2006.

[5]. W. Leonhard, Control of Electrical Drives. Springer-Verlag, 1985.

[6]. M. P. Kazmierkowski, R. Krishnan, and F. Blaabjerg, Control in Power Electronics: Selected Problems. Academic Press, 2002.

[7]. P. Vas, Sensor less Vector and Direct Torque Control. Oxford University Press, 1998. R.H.Park,Two Reactions Theory of Synchronous Machines. AIEE Transactions. Vol. 48, pp. 716–730, 1928.